Review

Materials and Life Science Experimental Facility at the Japan Proton Accelerator Research Complex I: Pulsed Spallation Neutron Source

Hiroshi Takada *, Katsuhiro Haga, Makoto Teshigawara, Tomokazu Aso, Shin-Ichiro Meigo, Hiroyuki Kogawa, Takashi Naoe [ORCID]**, Takashi Wakui, Motoki Ooi, Masahide Harada and Masatoshi Futakawa**

J-PARC Center, Japan Atomic Energy Agency, Tokai, Ibaraki 319-1195, Japan; haga.katsuhiro@jaea.go.jp (K.H.); teshigawara.makoto@jaea.go.jp (M.T.); aso.tomokazu@jaea.go.jp (T.A.); meigo.shinichiro@jaea.go.jp (S.-I.M.); kogawa.hiroyuki@jaea.go.jp (H.K.); naoe.takashi@jaea.go.jp (T.N.); wakui.takashi@jaea.go.jp (T.W.); ohi.motoki@jaea.go.jp (M.O.); harada.masahide@jaea.go.jp (M.H.); futakawa.masatoshi@jaea.go.jp (M.F.)

* Correspondence: takada.hiroshi90@jaea.go.jp; Tel.: +81-29-282-6424

Abstract: At the Japan Proton Accelerator Research Complex (J-PARC), a pulsed spallation neutron source provides neutrons with high intensity and narrow pulse width pulse to promote researches on a variety of science in the Materials and Life Science Experimental Facility (MLF). It was designed to be driven by a proton beam with an energy of 3 GeV, a power of 1 MW at a repetition rate of 25 Hz, that is world's highest power level. It is still on the way towards the goal to accomplish the operation with a 1 MW proton beam. In this review, distinctive features of the target-moderator-reflector system of the pulsed spallation neutron source are presented.

1. Introduction

The Japan Proton Accelerator Research Complex (J-PARC) is a multi-purpose research facility complex consisting of 3 accelerators and 4 experimental facilities. The Materials and Life science experimental Facility (MLF) is one of experimental facilities of J-PARC, having muon and neutron facilities. At MLF, a pulsed spallation neutron source was built to provide high-intensity and high-quality neutron beams for cutting-edge research on a variety of materials science [1]. It was designed to receive a 3 GeV proton beam with 333 μA, the power of 1 MW, at a repetition rate of 25 Hz. The proton beam is accelerated up to 0.4 GeV by a linac and accumulated in 2 short bunches, and then accelerated up to 3 GeV in the Rapid Cycling Synchrotron (RCS), resulting to have a structure of a 150 ns bunch width with a spacing of 600 ns per 1 macro pulse. The beam extracted from the RCS is delivered to the spallation neutron source through the 3 GeV RCS to Neutron Facility Beam Transport (3NBT) [2–4].

The linac comprises a volume-production type of H⁻ ion source, a 50-keV low energy beam transport (LEBT), a 3-MeV, 324-MHz Radio-Frequency Quadrupole (RFQ) linac, a 50-MeV, 324-MHz Drift-Tube Linac (DTL), a 200-MeV, 324-MHz Separated DTL (SDTL), and a 400-MeV, 972-MHz high-energy linac [5]. The RCS was designed to have a lattice with three-fold symmetry, resulting in three long straight sections [5]. One is dedicated to the long RF acceleration section, another to the injection and collimation, and the last to the extraction. In the RCS, 24 bending magnets, 60 quadrupole magnets and 18 sextqupole magnets were installed. The innovative development of the accelerating cavity loaded with magnetic alloy [6] enabled to solve the issue of powerful RF accelerating system.
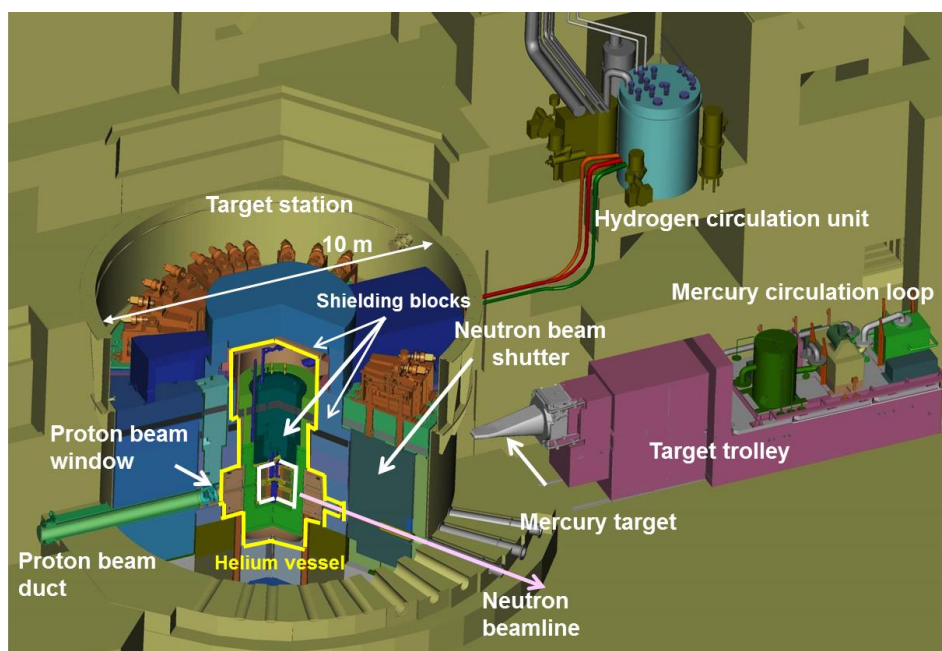
For the pulsed spallation neutron source, liquid metal, mercury was employed as the target material because it has advantages in producing neutrons with its large atomic number of 80 and high weight density of 1.36×10^4 kg/m^3 via proton induced spallation reactions, and high heat removal capacity. Energies of spallation neutrons are in the MeV regime, hence they have to be slowed down to the cold neutron (meV) region suitable for neutron scattering experiments. For that purpose, liquid hydrogen (20 K) was selected as the moderator material. A mercury-target-moderator-reflector system was designed carefully in view of maximizing the intensity of neutrons and making the pulse shape as narrow as possible. As a result, 3 types of moderators, coupled, de-coupled and poisoned moderators were optimized to use 100% para-hydrogen.

Figure 1 shows a cutaway view of the spallation neutron source. The high radiation zone including the target, the three moderators in wing configuration, and the reflector and central shielding are placed inside a helium-filled vessel. The helium vessel with its inactive helium filling prevents the production of corrosive gases such as O_3, NO_x and acts as protective boundary against possible spills of mercury and light water in case of serious failure incidents. The moderators' side surfaces are the origins of the neutron beamlines. Since 2 sides of each moderator are used as viewed surfaces by the neutron beamlines, there are 6 origins, and 23 neutron beamlines are arranged from those origins. Outside the helium vessel, a neutron beam shutter made of steel with 2 m in length and 4 m height was installed on each neutron beamline. It moves vertically to open and/or close the beamline with a 1-m stroke.

The target, moderators and reflector are highly damaged by a high-power operation at 1 MW. Therefore, they must be replaced by full remote-controlled tools before the estimated end of lifetime. Since the lifetime of the target vessel is much shorter than that of the moderators and reflector, different access ways, horizontal access for the target vessel replacement and vertical access for the moderator-reflector system replacement, were selected. This enables us to replace the mercury target vessel without handling the moderators and reflector. The shielding structure surrounding the target-moderator-reflector system, e.g., neutron beam shutter, was determined by three-dimensional Monte-Carlo simulations in which geometry of all components was exactly modelled [7]. In particular, neutron and/or photon streaming through the gap between the components installed side by side were estimated carefully to meet the shielding design criteria that the dose rate was less than 2.5 μSv/h at the biological shield surface. As a result, the diameter of the target station was determined as 10 m with additional heavy weight concrete with a thickness from 2 to 2.5 m as biological shield, while the height was set to 10 m including an open space of 1.8 m for the neutron shutter drive devices.

Outside the target station, 3 GeV proton beam transport line components were installed at 330 m length upstream of the target. A cryogenic hydrogen system composed of a helium refrigerator and a hydrogen loop is arranged on the high bay from which liquid hydrogen is provided to three moderators. A target system maintenance area is placed just downstream from the target station where the components are replaceable with remote handling tools. The moderators and reflector are transferred into this are on the way of the high bay in case of the replacement. The maintenance scenario for the used components is summarized in reference [8]. Furthermore, primary and secondary cooling system and an off-gas processing system were installed in the areas next to the target maintenance area.

Construction of mega-watt class pulsed spallation neutron source is a challenging work. The Spallation Neutron Source (SNS) [9] project at Oak Ridge National Laboratory (ORNL, Oak Ridge, TN, USA) that was aimed at operating with a proton beam power of 1.4 MW at 60 Hz had been started a few years earlier than J-PARC. The European Spallation Source (ESS, Lund, Sweden) [10], a 2.86 ms long proton pulse facility designed to be operated with a 5 MW proton beam at 2 GeV, is under construction in Lund, Sweden. The concept to use a mercury target with liquid hydrogen moderators was already adopted in the SNS. However, details of our design are quite different from SNS. This article focuses on designs of the mercury target system, the moderators and the cryogenic hydrogen system are focused. They are described in the Sections 2–4, respectively. Furthermore, outline of the 3NBT is given in the Section 5.

Figure 1. Cutaway view of the target station of pulsed spallation neutron source of the Japan Proton Accelerator Research Complex (J-PARC) with target trolley moved back to the service position.

2. Mercury Target System

2.1. Target Trolley

The target trolley is the carriage of the target vessel and the mercury circulation system as shown in Figure 2. It has a dimension of 12.2 m in length, 2.6 m in width and 4 m in height, and total weight of 315 tons and it installs the target vessel into the helium vessel for beam operation with enough radiation shielding behind against secondary particles generated via spallation reactions in mercury. For maintenance, it withdraws to the target maintenance area of hot cell (Maximum distance: 23 m). Radiation shield blocks made of iron and concrete provides most of the weight, through which many pipes such as mercury pipes and helium gas supply pipes penetrate. Behind the radiation shield, further iron blocks cover two mercury drain tanks and two spilt mercury tanks for shielding γ-rays emitted from radioactive spallation products in mercury in the drain tanks during the maintenance [1], and a trolley driving mechanism is mounted at the rear end. The mercury circulation system placed on the mercury system trolley comprises mercury pipings, a mercury pump, a heat exchanger, a surge tank, a gas supplying system and sensors.

In order to maximize the neutronic performance, the components are installed in the target station with minimum spatial gap. For example, the design gap between the neutron reflector housing and the target vessel was set to 8 mm considering the following assembling and positioning tolerances of those components; (1) the tolerance of the neutron reflector housing is 3 mm, (2) the manufacturing and assembling accuracy of the target vessel itself is 1 mm, (3) the positioning reproducibility of the target trolley is 1 mm, (4) positioning tolerance of the target vessel on the target trolley is 2 mm, and (5) an additional margin of 1 mm.
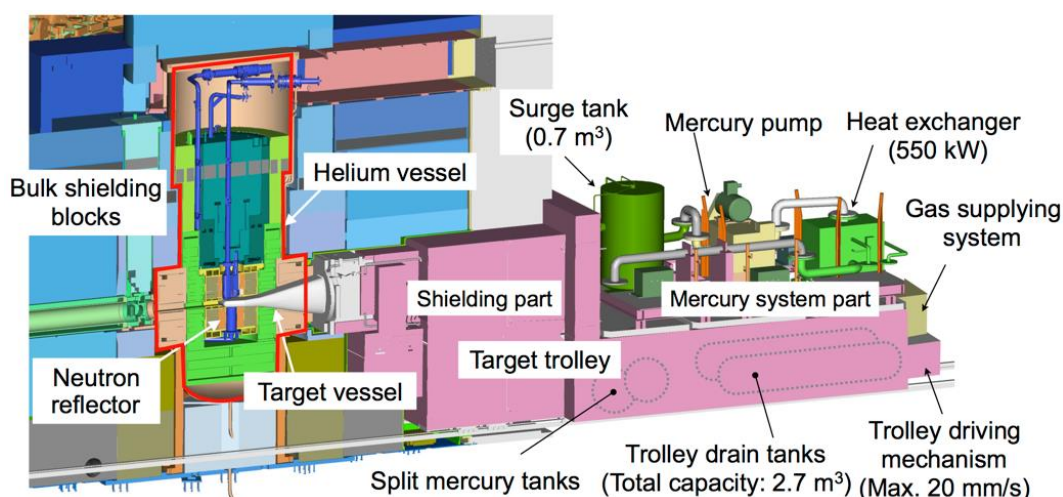
Figure 2. Layout of devices in the mercury target system mounted on the target trolley.

2.2. Mercury Target Vessel

Figure 3 shows photographs and schematic illustrations of the mercury target vessel. It comprises a mercury vessel and a double-walled water shroud covering the mercury vessel, which makes the target vessel a triple-walled structure. The forefront wall of the target vessel is called as the beam window on which proton beams are injected. The triple-walled structure prevents the mercury leakage to the outside in case of failure of the target beam window [11]. The mercury vessel is cooled by mercury flow, while the water shroud is cooled by water flowing through the double-wall gap. The interstitial space between the mercury vessel and the water shroud is filled with helium gas. In the mercury vessel, six flow vanes are placed in the mercury flow path to establish the "cross-flow", which indicates that mercury crosses the main part of the target in order to remove the heat generated by proton-induced spallation reactions in mercury as shown in Figure 3c. This cross-flow type (CFT) target vessel has definite advantages in terms of heat removal and mechanical strength. Mercury flow distribution in the CFT target, which corresponds to the heat generation distribution along the target length, enables efficient cooling of the spallation heat and small amount of mercury inventory. In addition, flow vanes are also designed as a reinforcement to ensure the enough mechanical strength of the vessel.

The inner structure arrangement of the target vessel was determined based on the results of thermal-hydraulic analyses, structural analyses and pressure wave analyses under the condition of 3 GeV, 1 MW proton beam injection. Abrupt temperature rise in mercury caused by the pulsed proton beam injection generates pressure waves. The pressure wave load and cavitation erosion induced on the beam window has been recognized as the critical issue for the target vessel design [12]. The original target vessel was designed on the condition that the proton beam profile is Gaussian distribution with a beam footprint of 130 mm × 50 mm. Recently the proton beam profile was changed to the beam footprint of 180 mm × 70 mm to moderate the pressure wave load on the beam window, decreasing the maximum heat generation rate down to 220 MW/m^3 from the former value of 668 MW/m^3. Furthermore, in order to increase the durability of the beam window against the cavitation erosion, the inner surface of the beam window was hardened by using carburizing method named Kolsterising®, Bodycote plc, Macclesfield, UK [13]. The bubble generator to inject gas micro-bubbles in mercury is installed in the target vessel to reduce the pressure waves. Details will be described in Section 2.3. Furthermore, a double-walled structure target with a narrow gap mercury flow channel of 2 mm in height at the beam window was adopted since 2013, aiming at mitigating the cavitation damage formation by increasing the mercury flow velocity and the narrow gap effect [14].
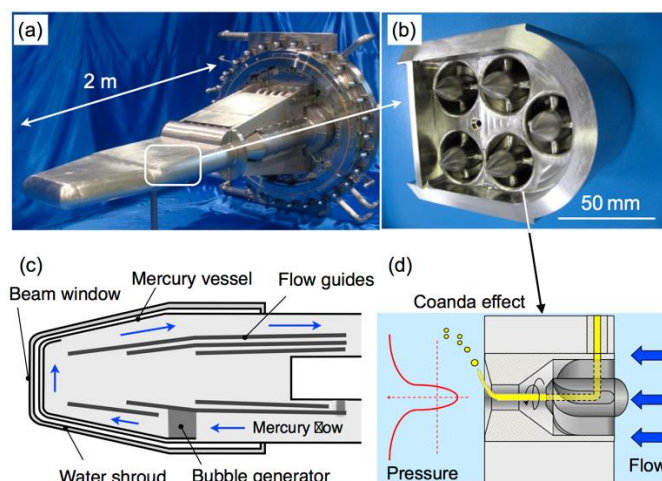
Figure 3. Photographs of target vessel (**a**) and bubble generator assembly (**b**), and their schematic views (**c**) and (**d**).

2.3. Microbubble Injection System

Currently, cavitation damage is considered to be the dominant factor to determine the service lifetime of the target vessel rather than radiation damage. Non-condensable helium gas micro-bubbles are effective to suppress the pressure waves in mercury which causes cavitation, because they absorb thermal expansion of mercury at the proton beam injection, and change kinetic energy of the pressure wave to thermal energy by their oscillation. Since pressure rising is very fast, e.g., the maximum pressure reaches to 40 MPa at 1 μs after the 1 MW proton beam injection, it is necessary to inject gas micro-bubbles less than 100 μm in diameter with a 0.1% volume fraction to mercury for effective pressure waves mitigation [15,16].

We developed a gas microbubble generator [17] for generating bubbles to satisfy the design condition mentioned above, and have installed it in the mercury target system with a closed-loop gas supply system in October 2012. Figure 3b,d show the photograph and schematic of the microbubble generator. Gas is injected from the center of the static swirler to make a gas column and brake down to the microbubbles owing to the shear force induced by the vortex-breakdown at the outlet of bubble generator. Multiple bubble generators with opposite swirl direction were placed alternately to prevent the bubble coalescence due to the bulk swirl flow.

The gas supplying system circulates the helium gas enclosed in the mercury loop as follows: helium gas flows from upper space of the surge tank to a compressor of gas supplying system and is pressurized, so that it could flow towards the bubble generator in the target vessel according to the differential pressure between those components. Double containment metal bellows compressor was selected for the gas supplying system to detect the gas leakage from internal bellows and to assure the containment of radioactive cover gas in it. The flow rate of helium gas was adjusted to be 1.5 L/min at standard condition with a flow control valve. Resultant helium gas fraction at the beam window of the target vessel was estimated to be about 1.5×10^{-4} under this flow condition.

2.4. Mercury Circulation System

As mentioned before, primary components of the mercury circulation system are the surge tank, the mercury pump, and the heat exchanger. The most important and challenging issue for this system design was that all the components should be maintained by remote handling. Though the system seems very simple in the figure, it is actually more complicated because a lot of devices such as valves, thin pipes, cables, flanges, connectors etc. are installed to the system, which are not shown in Figure 2. Thus, each component was devised and arranged on the target trolley, and so that it could be maintained easily by remote-handling. Table 1 summarizes primary specifications of each component.

The mercury circulation system will be operated with a mercury pressure of 0.5 MPa, with keeping this operational pressure by pressurizing the surge tank with helium gas. Type 316L stainless steel (316L SS) was chosen as the primary component material considering its corrosion and radiation resistant property. Inner diameter of the mercury primary piping is 143.2 mm and no valves are installed on the primary loop. Also, the mercury loop has neither strainer nor filter, because the surge tank is expected to serve the same function. Most of mercury compounds produced with spallation product or component of wall material in the system are solid and lighter than mercury itself, so they will be trapped in the surge tank as scum floating on mercury, which was demonstrated in a small mercury loop in our laboratory. In order to minimize the mercury piping erosion and prevent the mercury cavitation, the maximum mercury flow velocity was set to be less than 1 m/s. As a result, the operational mercury flow rate was determined as 41 m^3/h, which was equivalent to the mercury flow velocity of 0.7 m/s in the mercury primary piping. Based on the experimental data of erosion and corrosion by mercury flow, pipe wall thickness of 11 mm was chosen to have enough erosion and corrosion allowance for the designed facility life time of 30 years [18].

For circulating mercury, a permanent magnet rotating type induction pump (PM pump) is employed. The PM pump can be operated at a low risk springing a mercury leak because it has no seal parts. However, a large motor is required to generate sufficient flow rate on account of the low efficiency of the PM pump. Almost the total motor power is converted to the thermal heating in the PM pump, which should be removed by a heat exchanger in the mercury circulation system. Therefore, the PM pump was developed to reduce the thermal heating and to increase the flow rate of the mercury [19]. Figure 4 shows a schematic drawing of the PM pump. The dimensions of the pump are 0.8 m in length, 1.1 m in width, and 2.0 m in height, and total weight is 2.0 tons. In this pump, the mercury duct was made in a circular shape and rotating permanent 16 poles Sm-Co magnets were installed at the center of the duct to apply the Lorentz force, and the motor to rotate the permanent magnets was vertically set on the top of the pump to arrive at a compact PM pump design. Furthermore, the thickness of the duct wall and the duct width of the practical PM pump were carefully determined to assure the pump pressure to circulate mercury in required flow rate taking account of a power loss from the 90 kW motor for the thermal heating in the duct wall. The resultant duct is made from 316L SS with a diameter of 379 mm, a height of 340 mm, and an inner and outer thickness of 3 mm and 5 mm, respectively.

A double walled plate type heat exchanger of which parts are fully welded and fabricated together was adopted in order to reduce the possibility of radioactive mercury leak to the secondary loop. Helium gas is sealed in the double wall gap and mercury leak into the gap will be detected by monitoring the helium pressure change. The mercury is cooled down from 72 °C to 50 °C in this heat exchanger. The secondary coolant is light water with an inlet temperature of 35 °C and it is cooled in the cooling tower placed outside of the facility building.

Table 1. Primary specifications of mercury circulation system components.

| Name of Component	Specification
Mercury Pipe	Inner Diameter: 143.2 mm
	Wall thickness: 11 mm
Surge tank	Capacity: 0.7 m^3
Mercury pump	Type: Permanent magnetic type
	Rated flow rate: 41 m^3/h
	Discharge pressure: 0.5 MPa
Heat exchanger	Type: Double wall (All welded)
	Heat removal capacity: 600 kW (max.)
Flow Meter	Type: Venturi
	Measurement range: 0~60 m^3/h
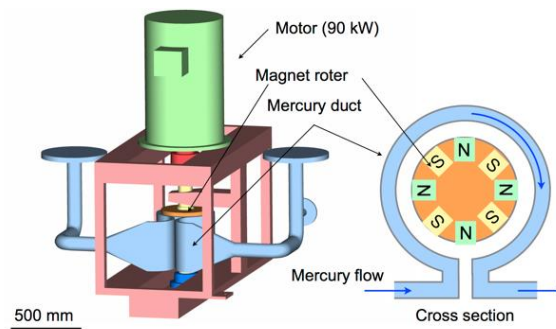
**Figure 4.** Schematic view of the permanent magnet rotating type induction pump (PM-pump).

2.5. Target Diagnostic System

In order to monitor the pressure wave-induced vibration of the target vessel at the proton beam injection, a non-contact and nondestructive diagnostic method is required to be used in the high-radiation environment [20]. To meet the requirement, a novel in situ diagnostic system using a laser Doppler vibrometer (LDV) was developed. Figure 5 shows the schematic drawing of the LDV diagnostic system. It comprises a retro-reflecting corner-cube mirror (reflective mirror) mounted on the upper surface of the target vessel, a mirror assembly, a laser light source and an avalanche photo diode as a laser light detector [21]. Laser light is emitted on the top of shielding plug placed above the target vessel and passes through the mirror assembly for 3.4 m and incident upon the reflective mirror on the target vessel. A He-Ne laser (wave-length: 632 nm) with a power of 2 mW was employed to have high coherence to improve the signal to noise ratio (S/N). The reflective mirror was fabricated out of a Au plate with a direct micro machining process to have high-reflectance of 56% and high-corrosion resistance.

Figure 6 shows the displacement velocity of the target vessel measured with LDV for the 310 kW proton beam injection with a power density of 2.8 J/cm^3/pulse [22]. It is obvious that the maximum displacement velocity observed after injecting proton beam decreased about one third by injecting gas micro-bubbles, and also decreased significantly in the time region after 2 ms.
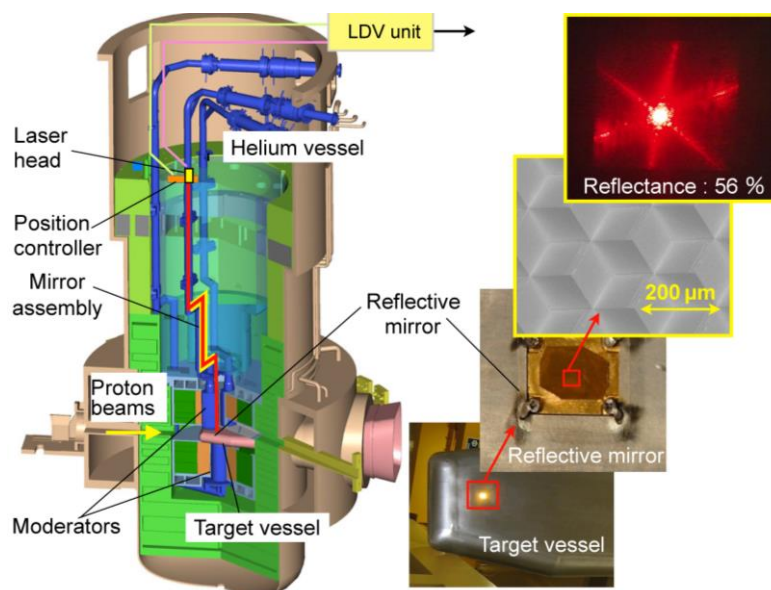
Figure 5. Target diagnostic system consists of the Laser Doppler vibrometer (LDV) installed in the helium vessel.
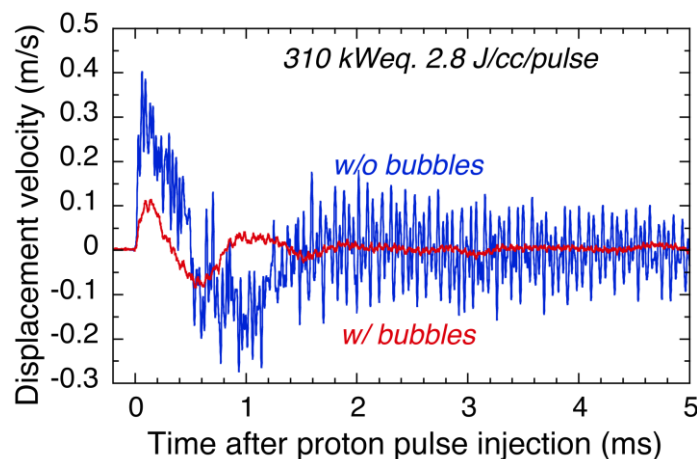
Figure 6. Time histories of the displacement velocity of the mercury target vessel measured with LDV system. Time 0 designates the proton impact on the target. Blue and red lines represent the data without and with injecting gas microbubbles, respectively.

2.6. Target Vessel Replacement

Once the target trolley is withdrawn into the maintenance room, the component replacement or repairing work is carried out using a power manipulator and some master-slave manipulators. Before removing the target, cover gas in the surge tank was transferred to an off-gas process system to reduce the radioactivity of gaseous radioactivity, especially ^{127}Xe and ^{3}H, accumulated in the cover gas. The transferred cover gas is stored in gas holders of the off-gas process system for about 12 months waiting for the decay of ^{127}Xe having half-life of 36.4 days, while ^{3}H is absorbed by a molecular sieve (synthetic zeolite) [23], and then released to the environment after checking the radioactivity. This gas transfer operation is repeated until the radioactivity of ^{127}Xe decreased down to 1/100 of its initial value, which is significantly below the allowable value even if the remaining ^{127}Xe in the loop is released through the stack of the building at any failure.

Figure 7 shows the procedure of the mercury target vessel replacement. A storage container is mounted on a target exchange truck. It supports the mercury target vessel after the connecters are disconnected and bolts are loosened. It is noted that mercury was drained into the drain tank installed beneath the target trolley prior to dismounting the target vessel. The used mercury target vessel in the storage container is moved to a storage room located below ground. The new mercury target vessel is installed to the target trolley in the reverse order of the target vessel removal. After the installation, airtightness test on all pipe connections is conducted to ensure their enclosure performance by filling helium into the circulation loop, where the criterion of airtightness is 10^{-6} Pa m^3/s. The helium filled into the loop is also transferred to the off-gas process system and then mercury is filled into the circulation loop from the drain tank.
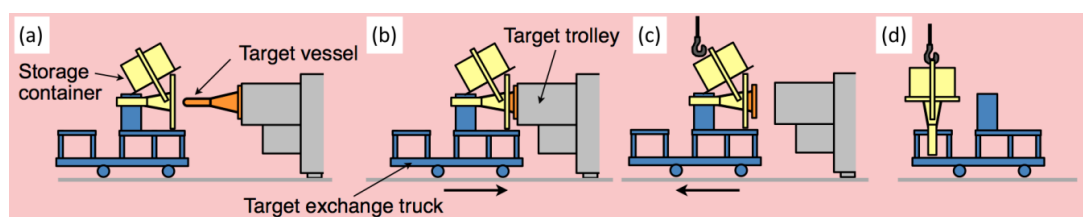
Figure 7. Procedure of the mercury target vessel replacement. (**a**) preparing the target exchange truck and the storage container; (**b**) insert the target vessel into the storage cask; (**c**) removing the target vessel from target trolley; (**d**) move the storage cask to the storage room. New target is set to the target trolley in the reverse order.

3. Moderator and Reflector Development

The wing geometry type, as shown in Figures 8 and 9, was adopted for the moderator-target arrangement where the horizontal proton beam is injected on the target. It was widely utilized at pulsed neutron sources, such as KENS facilities of High Energy Accelerator Research Organization (Tsukuba, Japan), ISIS of Rutherford Appleton Laboratory and the SNS of ORNL. At J-PARC, three moderators are arranged in total, two decoupled moderators (decoupled and poisoned) above the target and one coupled moderator below the target, respectively. The coupled moderator provides high peak intensity in neutron beam pulses by setting it on the target vessel closely without thermal neutron absorber. The decoupled moderator provides neutron pulses with short tails by adopting a thermal-neutron-absorber-material called decoupler although the neutron intensity is sacrificed somewhat with it. For poisoned moderator, a sheet made from thermal-neutron-absorber is installed inside the moderator vessel so that the neutron beam pulse could have both narrow width and short tail. Illustrations of the coupled moderator and the decoupled moderator are shown in Figures 10 and 11. The moderator specifications are listed in Table 2. The arrangement (upper or below) was chosen to separate the coupled moderator from the thermal neutron absorber area installed for two decoupled moderators, and to provide the neutron scattering instrument, reflectometer, with neutrons through a vertically inclined neutron beam line that is optimized to use the coupled moderator.

Resultant three moderators have following distinctive features: moderators were optimized to use para-hydrogen, giving highest neutronic performance, such as neutron intensity per pulse, especially for the coupled moderator,

1. high decoupling energy of 1 eV was achieved by adopting a Ag-In-Cd decoupler, providing short tail in the pulsed neutron beam emitted from the decoupled and poisoned moderators,
2. cut-off energy was extended up to 0.4 eV by adopting a cadmium poison sheet, resulting in sharper pulse width for the poisoned moderator.
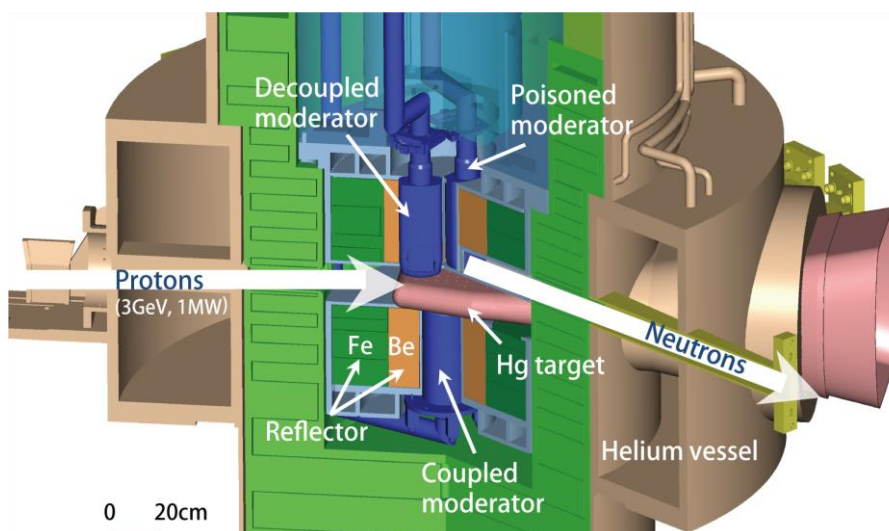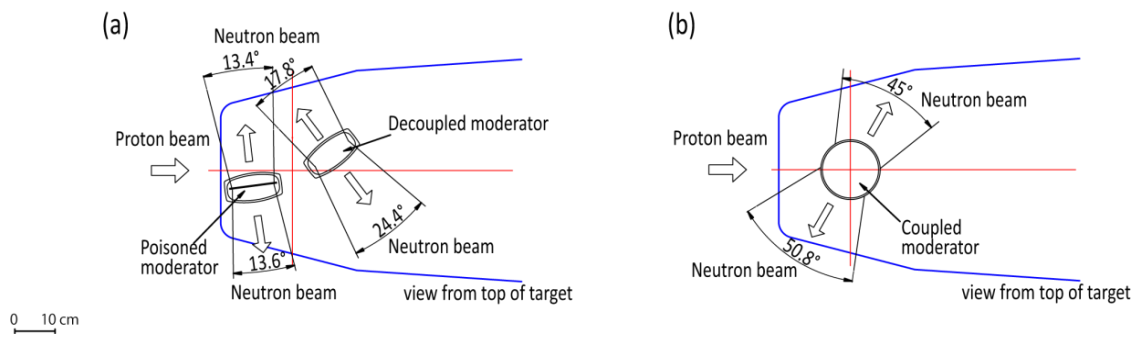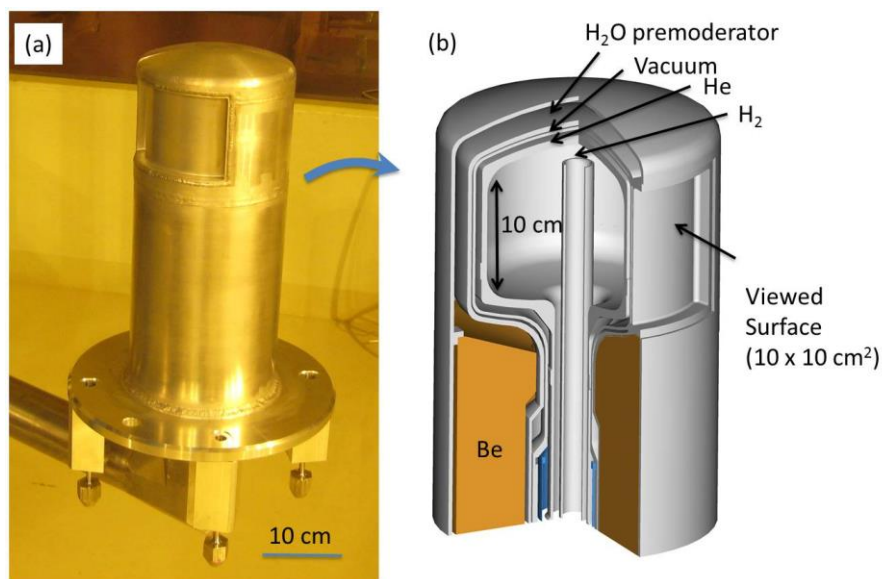

Figure 8. Cross sectional view of target-moderator-reflector.

Figure 9. (**a**) Locations of decoupled and poisoned moderators with respect to the target vessel; (**b**) Location of coupled moderator with respect to the target vessel. The directions and angles of neutrons extracted from each moderator surface to neutron beamlines are also shown.

Figure 10. (**a**) Photograph of coupled moderator; (**b**) Cutaway view of coupled moderator.
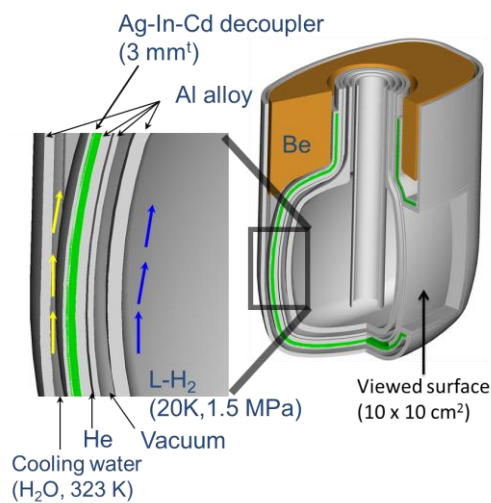
Figure 11. Illustration of inside structure of de-coupled moderator.

Table 2. Major specifications of moderators employed at J-PARC.

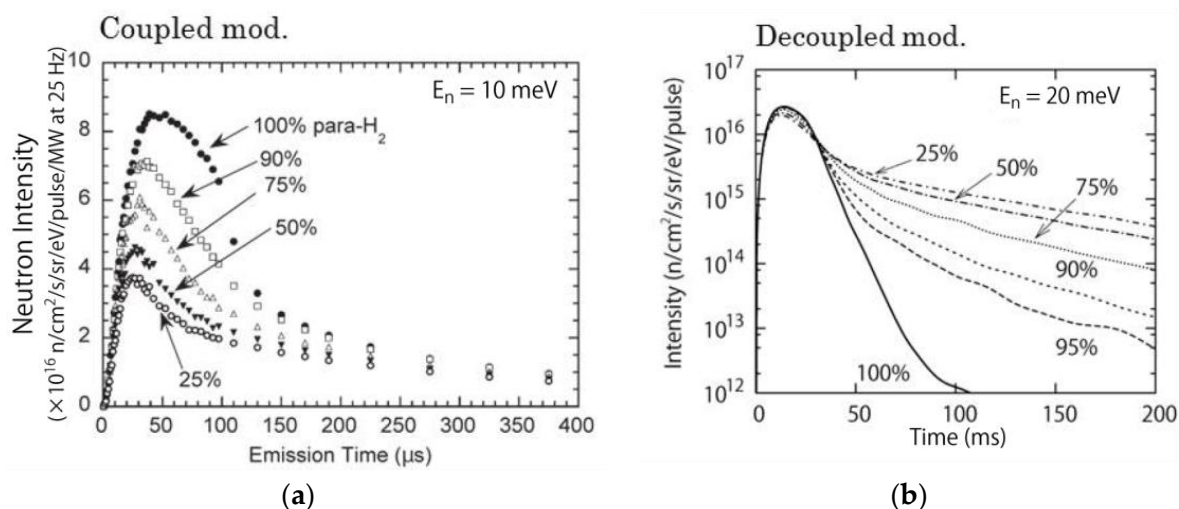| Moderator	Coupled	Decoupled	Poisoned
Beam extraction	Two-sided	Two-sided	Two-sided
Angular coverage	50.8°/45°	24.4°/17.8°	13.4°/13.6°
Main moderatow	H_2, 20 K, 15 atm	H_2, 20 K, 15 atm	H_2, 20 K, 15 atm
Shape	Cylindrical	Canteen	Canteen
Size	$\phi 14$ cm $\times 10^H$ cm	$13^W \times 12^H \times 6.2^t$ cm^3	$13^W \times 12^H \times 6.2^t$ cm^3
Premoderator	H_2O (1 cm^t)	Non	Non
Decoupler	-	Ag-In-Cd	Ag-In-Cd
Decoupling energy		1 eV	1 eV
Poison	-	-	Cd (1.3 mm^t)
Viewed surface	10×10 cm^2	10×10 cm^2	10×10 cm^2

H: Height; W:Width; t:thickness.

To obtain an optimum for the target-moderator-reflector layout in view of enhancing neutron production efficiency, design parameters such as the proton beam footprint on target, relative longitudinal moderator position to the target and distance between target and moderator were assessed by neutronics calculations. As a result, the proton beam footprint with 13×5 cm^2 at the target front was determined. It was also estimated that intensity of the slow neutron emitted from the coupled moderator was maximum at 15.5 cm downstream from the target front [1,24,25] which determined the coupled moderator position with respect to the target. The distance between target and moderator were set to 8 mm taking account of tolerances in component fabrication and installation as mentioned in Section 2.1.

Liquid hydrogen has been identified as the only practical cold moderator material for the moderation of MW-class high-intensity sources, considering the irradiation damage [26–28]. Since it has a relatively low hydrogen density (ca. on half of solid methane), it has not been used widely in view of enhancing cold neutron intensity in the spallation neutron source so far. In this design, we focused on the para-hydrogen, one of two isometric forms of liquid hydrogen, to improve the neutronic performance, because it would give shorter tails on the resulting neutron pulses due to its low cross section blow 14.5 meV [29]. On the other hand, it was estimated that neutrons leaked more quickly in the slowing down process. To overcome the drawback of hydrogen for an MW-class energy source, extensive optimization studies have been conducted [30–40]. Especially for the coupled moderator, unique optimization to have large sized cylindrical shape coupled with optimized water pre-moderator gave higher neutron intensity [36,37], and so could provide the highest neutron intensity per pulse in the world [40]. It was also concluded that para-hydrogen fraction plays an important role of neutronic performance [37,40]. This benefit of para-hydrogen moderator is taken into account in the present high power neutron source projects of the ESS [41,42] and the second Target station design at SNS of ORNL [43].

As mentioned above, the neutronic performance, particularly pulse shape, strongly depends on the para-hydrogen fraction [35,38], as shown in Figure 12. E. B. Iverson and J. M. Carpenter calculated the irradiation effect on the para-hydrogen to ortho-hydrogen conversion under the high neutron irradiation environment [44,45]. Changes in the pulse shape of the para-hydrogen fraction were measured at the neutron source at Hokkaido University Electron Linac Facility and the Manuel Lujan Jr. Neutron Scattering Center of the Los Alamos National Laboratory [46,47]. However, there was no clear indication of the irradiation effect on para-hydrogen to ortho-hydrogen conversion because the neutron intensity was too weak at the Hokkaido University facility and the pulse shapes emitting from the moderator were only measured according to the elapsed proton beam operation time in the Los Alamos experiment. Then, we developed a method of sampling gaseous hydrogen from the circulating hydrogen in the hydrogen loop (1.5 MPa, 20 K) under high neutron irradiation at J-PARC, and measure the para-hydrogen fraction with a Laser Raman spectroscopy. The measured para-hydrogen fraction was consistent with the equilibrium level of para-hydrogen at 20 K (99.8%) at

the 300 kW beam operation because a Fe(OH)$_3$ catalyst worked well in the loop. The measured pulse shape at 300 kW was also in good agreement with the calculated result for the 99.8% para-hydrogen [48].


Figure 12. (**a**) Para-hydrogen concentration dependence on pulse shapes for the coupled moderator [30] and (**b**) the de-coupled one [38].

For the decoupled and poisoned moderators, a thermal neutron absorber acting as decoupler as shown in Figure 11, is installed around the moderator except for neutron beam extraction window, resulting in a short decay time in neutron beam pulse. Higher cut-off energy, which is called decoupling energy (E_d), gives a shorter decay time [49]. At J-PARC, neutron beam users required at least 1 eV decoupling energy for high-resolution neutron scattering experiments in the design stage. At the ISIS of Rutherford Appleton Laboratory (160 kW neutron source), boron-based material, such as sintered boron carbide (B$_4$C), was previously utilized to obtain a high decoupling energy (over 1 eV) with controlling its thickness. However, this cannot be used for MW-class sources because of the helium embitterment caused by the (n, α) reaction. In order to realize a high decoupling energy of 1 eV, we focused on a Ag–In–Cd alloy [50], a combing elements of different resonance energy absorption to yield an effective decoupling energy of 1 eV. Ag-In-Cd sheathed with stainless steel is already utilized for the control rod of PWR (pressurized water reactor). In view of heat removal and corrosion protection, however, there was the issue that the Ag-In-Cd plate has to be bonded to the Al alloy (A5083), the structural material of a moderator and reflector. We succeeded to implement Ag-In-Cd alloy into the moderator-reflector as a decoupler by adopting HIP (Hot Isostatic Pressing) method [49,51,52]. In order to validate neutronic performance of the Ag-In-Cd decoupler, the pulse shape was observed in the rise and tail part of the Bragg peaks. As shown in Figure 13, the measured and calculated time structures of the neutron pulses were in good agreement [40]. However, the Ag–In–Cd decoupler has a disadvantage that highly residual radioactivity is generated especially by the production of ^{108m}Ag (half-life of 418 years).

We proposed a new idea [53] to reduce the potential risk of high residual radioactivity of AIC. It was that Au replaced silver in the Ag-In-Cd composition. As a result of neutronic calculation considering the component change accompanied with accumulation and decay of residual nuclides, Au-In-Cd could reduce the residual radioactivity by three orders of magnitude than Ag-In-Cd without sacrificing neutronic performance [53]. We also adopted HIPing method to implement the Au-In-Cd decoupler to the next moderator-reflector fabrication [54–56]. The next moderators with the Au-In-Cd decoupler are under fabrication.
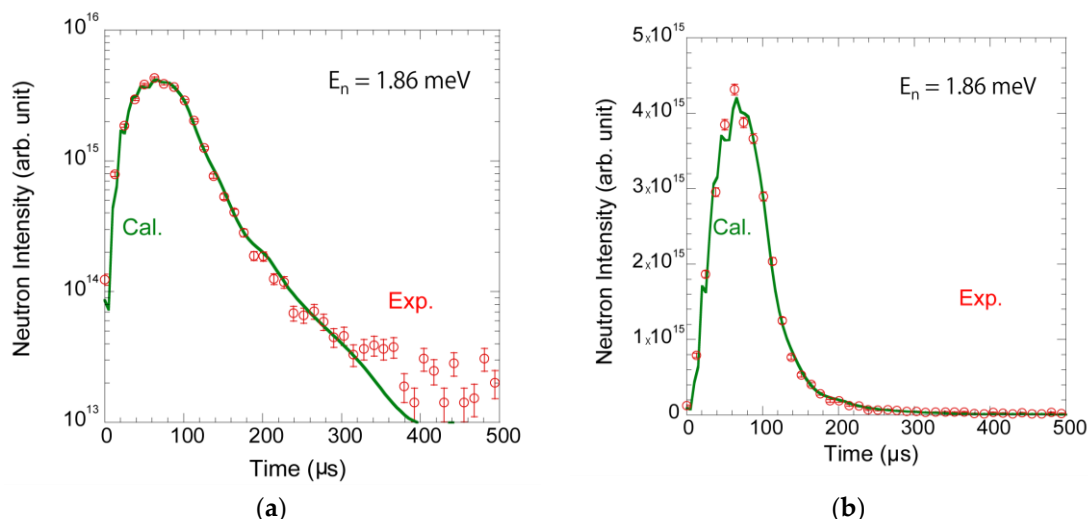
Figure 13. Measured and calculated neutron pulse emitted with 1.86 meV from decoupled moderator [40]. Graph is shown by logarithmic scale (**a**) and linear scale (**b**) in vertical axis. Open circle and solid line represents measured data and calculated results, respectively.

For the poisoned moderator, a Gd sheet has been widely used as a poison material. It was adopted at the Intense Pulsed Neutron Source (IPNS) in Argonne National Laboratory (Chicago, IL, USA), ISIS, and KENS, and is also in use at SNS. However, we attempted to use a Cd poison [39] thinking of two advantages. One is a higher cut-off energy than Gd, leading to make a sharper pulse width at higher neutron energies up to 0.4 eV, and the other is a weaker resonance capture leading to make the intensity penalty with thicker poison plate much smaller. By optimizing the Cd based poisoned moderator, actually outstanding performances of the world's highest resolution [40], 0.035% in $\Delta d/d$ was obtained at the super high-resolution powder diffractometer (SuperHRPD) [57] with long neutron flight path of 94.2 m, where d is the lattice-spacing of the Si-400 reflection at 4.628 Å^{-1} . The diffraction pattern obtained at the SuperHRPD is shown in Figure 14.
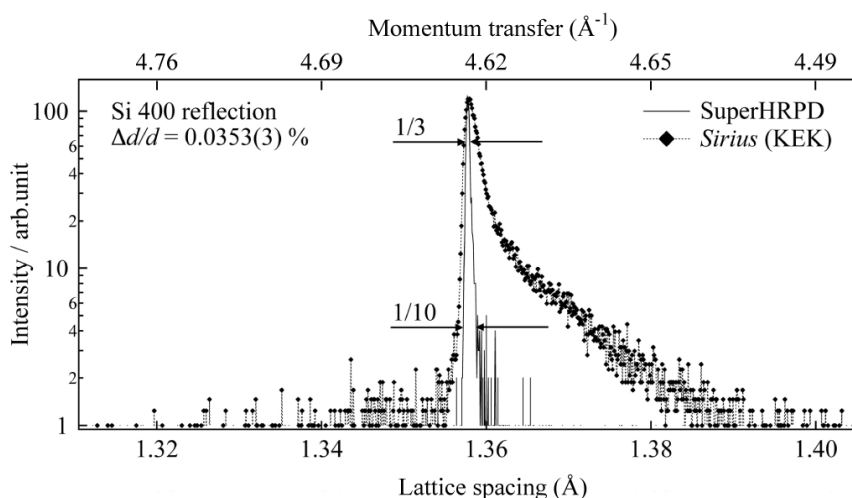
Figure 14. Comparison of neutron diffraction data for a silicon sample measured at super high-resolution powder diffractometer (SuperHRPD) (solid line) with those obtained at Sirius (dots) [40].

4. Cryogenic Hydrogen System

The cryogenic hydrogen system plays the role of providing the three moderators with cryogenic hydrogen continuously. It was estimated that several kW of heat was generated in the moderators

through nuclear heating at the 1 MW operation. This required the cryogenic system to have a kW-power. Forced-flow circulation cooling is also adopted to maintain the temperature of the moderators at 20 K regime and to attain small temperature difference between the inlet and the outlet of the moderator. The design of the system configuration, the specification of the components, and the physical layout are introduced as follows [58].

4.1. Design Requirements

The hydrogen moderator makes fast neutrons generated at the mercury target slow down to cold neutrons. The cryogenic system was designed to have following performance:

(1)   Average temperature at the moderators is kept less than 20 K at 1.5 MPa in order to achieve constant density.
(2)   Temperature difference between the inlet and the outlet of moderators is kept less than 3 K to prevent hydrogen density fluctuation.
(3)   Para-hydrogen concentration of the moderators is kept more than 99% for the neutronic performance that helps to slow down to cold neutrons.

From the viewpoints of safety, the following additional requirements were taken into account:

(4)   In order to reduce hazard potentials, it is necessary to minimize the inventory of hydrogen in the system.
(5)   Blanket structure with inert gases needs to prevent the hydrogen leakage to the outside from the system and to prevent air from entering the system.
(6)   Hydrogen vent line is required to release hydrogen safely when the refrigerator operation stops and any off-normal event takes place.

To meet the requirement of the item (4), we designed the cryogenic system comprising a hydrogen circulation system with the moderators and a helium refrigerator to cool it, because the helium refrigerator had been widely used in recent years. In order to satisfy the operational temperature condition (1), we decided to flow the cryogenic hydrogen in parallel to the three moderators. Since the hydrogen circulation system is a closed loop as a refrigerator, a pressure control system is required to compensate a large pressure change. If there is no control of pressure, the pressure change of about 3.7 MPa takes place at the moment that the accelerator beam is turned on and/or off at the 1 MW operation. Table 3 shows the nuclear heating power in the moderators and their vessels estimated by the neutronic design study. Based on these conditions and requirements, process flow of the cryogenic hydrogen system was calculated by solving mass and heat balance at the components to determine the sizing and the specifications. It is noted that we have to design, operate and maintain this system according to the Japanese regulation, High Pressure Gas Safety Lows.

Table 3. Estimated nuclear heating power deposited on each moderator at 1 MW proton beam.

	Coupled Moderator	Decoupled Moderator	Poisoned Moderator	Total
Volume (L)	1.54	0.97	0.97	3.84
Nuclear heating in hydrogen (W)	946	467	442	1855
Nuclear heating in vessel (W)	793	519	584	1896
Total heating in the moderator (W)	1739	986	1026	3751

4.2. Design of the Cryogenic Hydrogen System

4.2.1. System Configuration and Specification of the Main Components

A schematic configuration of the cryogenic hydrogen system is shown in Figure 15. It comprises a hydrogen circulation system to cool high-energy neutrons at the moderators and a helium refrigerator

system to cool hydrogen in the hydrogen circulation system. Figure 16 shows the arrangement of the cryogenic hydrogen system in the Materials and Life Science Experimental Facility (MLF) building. The compressor and related equipment, the cylinder storage for gas supply are placed outside the building. The cold box is arranged as close as possible (within 10 m) to the hydrogen circulation system to minimize the heat loss. The moderators are located at the center of the neutron source station and connected with the hydrogen circulation system with hydrogen transfer tubes of about 14 m length. They are able to be removed from the transfer tube with a coupler on top of the helium vessel in case of the replacement.
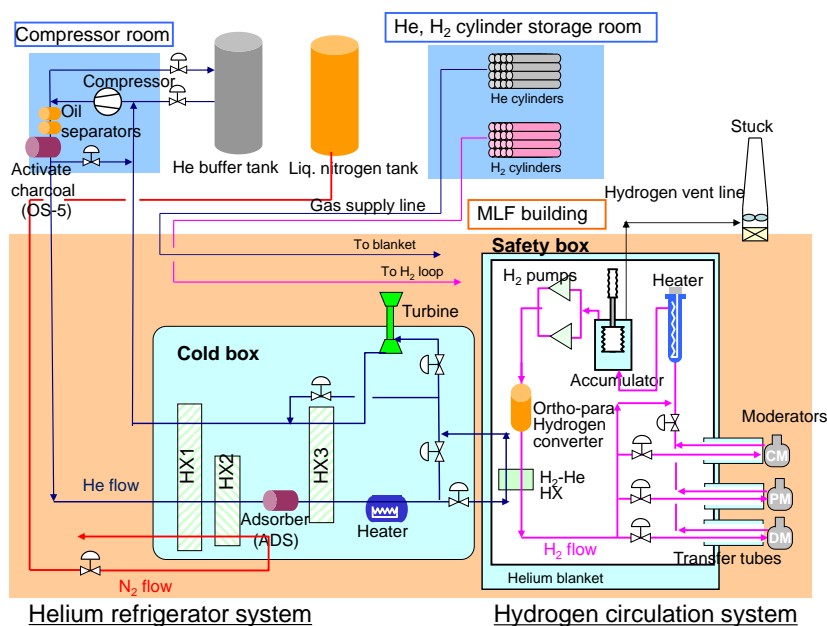
Figure 15. Schematic configuration of the cryogenic hydrogen system employed for pulsed neutron source of the Japan Proton Accelerator Research Complex (J-PARC).
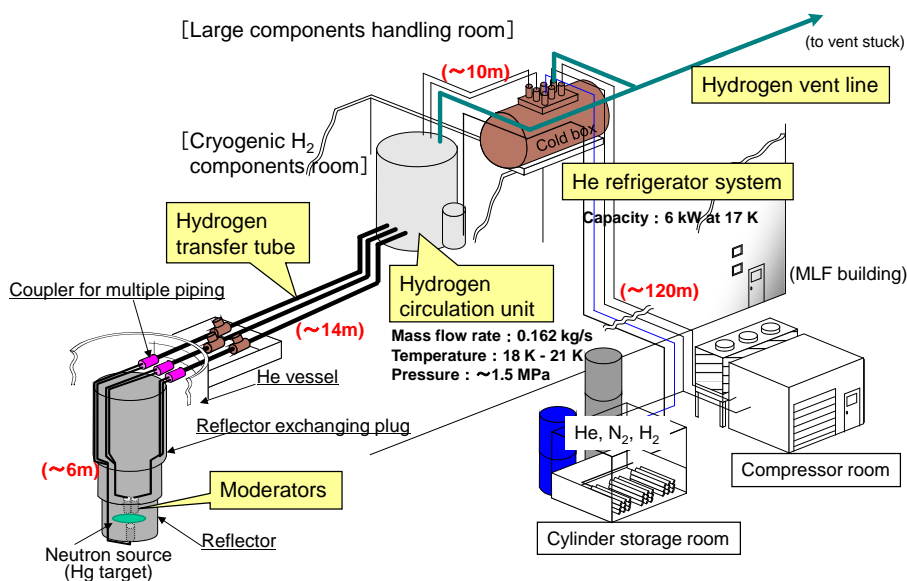
Figure 16. Illustration of cryogenic system component arrangement in Materials and Life Science Experimental Facility (MLF) building.

4.2.2. Helium Refrigerator System

The helium refrigerator system comprises a helium compressor, oil separators including an activated charcoal as an oil adsorber, a helium buffer tank and a cold box containing three heat exchangers, an adsorber, heater and turbine in the vacuum vessel. Table 4 summarizes specifications of the main components. They were determined based upon the results of the process flow calculation for the helium refrigerator system. The helium-refrigerator's refrigerating power at 17 K is specified to be around 6 kW in which a margin of 17% for the estimated total heat load is considered. In the helium refrigerator, an expansion turbine is located after the He-H_2 heat exchanger so as to keep hydrogen pressure to be 1.6 MPa in the helium part that is higher than the pressure of less than 1.5 MPa in the hydrogen part, enabling to prevent hydrogen leak into the refrigerator. Moreover, a heater installed prior to the He-H_2 heat exchanger keeps the hydrogen outlet temperature of the heat exchanger in constant.

4.2.3. Hydrogen Circulation System

The hydrogen circulation system circulates the cryogenic hydrogen through the three moderators and removes the heat generated in the moderator. It is made up of a He-H_2 heat exchanger, two hydrogen pumps, an Ortho-Para hydrogen converter, an accumulator and a heater. Those components are contained in a vacuum vessel, called safety box, covered by a helium blanket. Table 4 summarizes specifications of those components. The absorbed heat is transferred to the helium refrigerator through the He-H_2 heat exchanger.

The hydrogen pump is designed to get the mass flow rate of 0.162 kg/s with a pump head of 0.12 MPa at the rated condition [59]. It is an essential component to ensure reliable operation. Two pumps with the same specification are arranged in parallel and operated simultaneously with 50% of the load, respectively, and so have redundancy to continue operation with single pump with a 100% load even if either pump has failed.

The Ortho-Para hydrogen converter plays the role of keeping para-hydrogen concentration at more than 99% in the moderators in terms of providing superior neutronic performance. It was designed that the about 2% of ortho-hydrogen, which was converted from the para-hydrogen by the neutron irradiation in the moderator during the operation, is immediately converted to para-hydrogen through the converter. Our cryogenic system is the first device to install the Ortho-Para hydrogen converter among MW-class spallation neutron sources in the world.

A heater and an accumulator are installed as the pressure control devise to compensate large pressure fluctuations generated in the closed loop of the hydrogen circulation system. The heater performs an active control for thermal compensation, and the accumulator plays a role of passive volume control [60]. This is also the first time to use them together in the cryogenic system in the world. Present pressure control device enables the heater power to be smaller than the case with only the heater, and the hydrogen inventory to be smaller than the case controlled with only the accumulator.

4.2.4. Hydrogen Vent System

The hydrogen vent system is a specific apparatus. Inert gas, such as helium or nitrogen, always purges inside of the vent line to avoid air ingress into it. When the operation of this refrigerator is completed or stopped by an off-normal event, entire hydrogen in the system is safely released to the outside with inert gas.

Table 4. Specifications for main components of the cryogenic system.

Helium Refrigerator System	
Cold box	Type: Helium Brayton cycle Refrigeration capacity: 6000 W at 17 K Supply pressure: 1.6 MPa Liquid nitrogen consumption: 103 L/h
Helium compressor	Type: Oil injection screw compressor Suction/Discharge pressure: 0.31/1.7 MPa Mass flow rate: 0.285 kg/s Motor ratings: 690 kW
Hydrogen Circulation System	
Hydrogen circulation pump	Type: Centrifugal pump Inlet temperature: 19 K (available for 300 to 17 K) Inlet pressure: 1.5 MPa (available for 0.5 to 1.8 MPa) Mass flow rate: 0.162 kg/s Pressure head: 0.12 MPa (at 0.162 kg/s) Revolution: 30,000 rpm to 60,000 rpm
Ortho-Para hydrogen convertor	Catalyze: Iron hydroxide ($Fe(OH)_3$) Outlet Ortho-Para concentration: 99.0% Catalyst filling volume: 35 liter
Pressure control system Accumulator Heater	Type: Bellows structure (Inner welding bellows, Outer molding bellows) Size: ϕ310/350 mm (Inner bellows), ϕ59/80 mm (Outer bellows) Design pressure: 2.1 MPa Variable volume: 3.5 L Type: Sheath heater with baffle plate Power: Max. 7 kW
Heat exchnger	Type: Aluminum plate fin Size: W200 × H120 × L700 mm Temperature: H_2 22 (in)/18 (out) K, He 17 (in)/20 (out) K

5. Proton Beam Transport

5.1. Overview of the Proton Beam Transport

Figure 17 shows a plan view from the 3 GeV Rapid Cycling Synchrotron to the MLF building. In the MLF building, the Muon Science facility (MUSE) [61,62] is arranged upstream of the spallation neutron source, where a 2-cm-thick carbon graphite target is used for the muon production at 33 m upstream of the neutron production mercury target in a cascade scheme. The proton beam loses about 6.5% by the nuclear interactions at the graphite target. The spread angle of the 3 GeV proton beam scattered at the graphite target is estimated as 1.25 mrad. Considering this beam characteristics, the beam optics from the muon production target to the neutron production target was designed that the beam loss could be suppressed less than 1 W/m at the 1 MW operation. It is observed further beam loss of about 1.5% between the muon production and the neutron production targets. The present cascade target scheme is thought to give an advantage over a separated target scheme, because time sharing of the delivered proton beam to the neutron and muon targets would provide only 50% of the source strength to the respective user community. The 3NBT has been operated for eight years since it delivered the very first proton beam pulse to the neutron source in 30 May 2008. In 2015, for the first time, single bunches of the 1-MW-equivalent proton beam pulse were delivered to the neutron production mercury target without significant beam loss in the accelerator study conducted in January 2015. Following this study, in April 2015, proton beam power for the user program was set to 500 kW at 25 Hz operation.
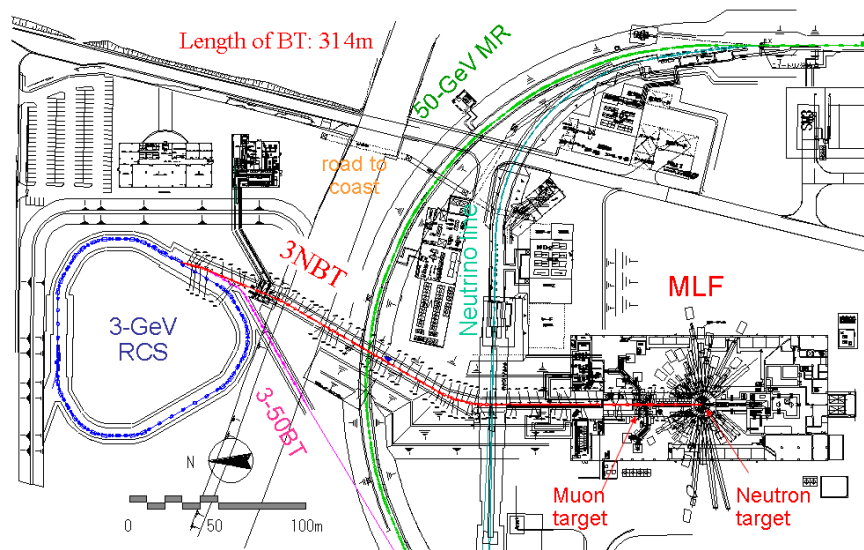
Figure 17. Plan view of the 3 GeV Rapid Cycling Synchrotron (RCS), the 3 GeV RCS to Neutron facility Beam Transport (3NBT) and the MLF at J-PARC.

5.2. Instruments for Beam Transport to Target

5.2.1. Magnets for Beam Transport

Since an uncontrolled high-power proton beam easily activates the beam transport equipment, a small beam loss rate is required in view of the instruments maintenance. In J-PARC, criterion for the beam loss was set as 1 W/m considering handling the instruments by hands on access. In order to deliver high intensity beam with very small beam loss, a careful design of the magnet, high precision and stable power supplies are essential. Also, it is important to align beam line components with high precision. Therefore, we routinely have been performing geometrical survey and alignment with a high precision laser tracker. Table 5 shows the specification of the magnets utilized for the 3NBT. Since high radiation environment is generated by the beam loss during the beam transport, it was required for the magnets to have high radiation resistance. Especially at the muon production target, large beam loss of about 6.5% is expected because of the nuclear interaction of proton beam with target nuclei. The insulator for the magnets installed around the muon target was carefully designed because an ordinary insulator such as polyimide used for coils will lose its insulation performance in the radiation environment. In the end, mineral insulator cable (MIC) made of MgO was utilized considering its high radiation resistance [63], enabling the absorbed radiation dose larger than the acceptable limit for polyimide of 400 MGy. It is also noted that the magnets around the muon production target can be replaced by remote handling if necessary in case of failure. They could be re-aligned on the exact position with an alignment pin installed at the bottom of the magnet.

Table 5. Specifications of magnet used in beam transport for spallation neutron source.

Magnet Type	Dipole for Bending	Quadrupole		Dipole for Sterling		Octupole
Insulator	Polyimide	Polyimide	MIC	Polyimide	MIC	Polyimide
Installed numbers	9	51	3	45	2	2
Aperture (mm)	160	220~300	260	200~300	260	300
Field or gradient	1.1~1.5 T	6~8 T/m	8 T/m	0.06 T	0.08 T	800 T/m^3
Field uniformity	5×10^{-4}	3×10^{-3}	3×10^{-4}	2×10^{-2}	2×10^{-2}	
and region (mm)	100	102~140	123	100	100	
Total weigh (t)	14~20	5~38 *	38 *	0.5~56 *	56 *	6

* Including shielding plug around muon production target. MIC: mineral insulator cable.

5.2.2. Proton Beam Monitor

In order to measure the characteristics of the proton beam, a diagnostic system with a Multi Wire Profile Monitor (MWPM), shown in Figure 18, was developed. Principle of the MWPM is simple that it measures the amount of electrons emitted by the interaction of the beam at the wire [64]. As a sensitive wire material, tungsten wire is generally selected because it emits a large amount of electrons and its melting point is so high. In the present system, however, SiC was chosen considering its high radiation resistance that can stand for the radiation damage up to 80 displacement per atom (DPA). Considering the high-intensity proton beam, proton beam loss at the MWPM is another important factor in selecting the material suitable for the wire. Since the Rutherford scattering of protons by target atom is proportional to the square of the atomic number, material with a low atomic number, such as SiC, has an advantage to reduce the beam loss.

Along the beam transport line, 15 sets of movable MWPMs were placed to measure the beam profile. The MWPM frame installed 31 wires of SiC with a spacing pitch of 6 mm in horizontal and vertical direction, respectively, where the SiC wire has a tungsten core of 0.01 mm covered with 0.15 mm of SiC. The wire frame was made of aluminum oxide with purity more than 95% to have enough high radiation resistance. The MWPM frame with wires is placed in the vacuum chamber made of titanium, which has good vacuum characteristics and low activation. In order to avoid unnecessary irradiation of the wires, the frame can retract and moves like pendulum motion. During the profile measurement, the beam loss is caused by the interaction at wires, which can be utilized to calibrate the beam loss monitors as well. When the amount of the beam loss exceeds the allowable value, the beam is stopped automatically by the interlock system called Machine Protection System (MPS) [65]. The beam loss monitors placed at all of quadrupole magnets, where the width of the beam becomes relative large. For the beam loss monitor, proportional counter and scintillation counter were selected. All of monitor information is acquired through Experimental Physics and Industrial Control System (EPICS) [66] and stored data base for each shots of beam [67]. From the information of beam orbit and width, the beam parameter such as profile on the target is adjusted by the Strategic Accelerator Design code system (SAD) [68] with several shots of beam.
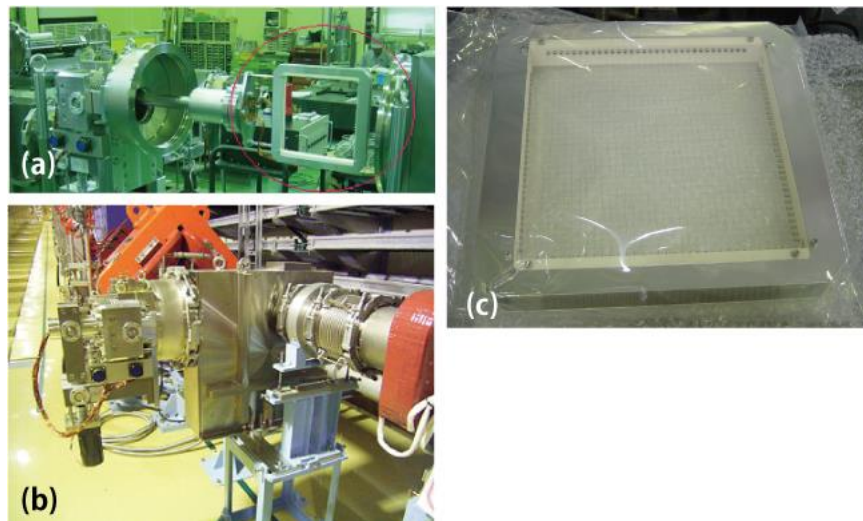

Figure 18. Photographs of Multi Wire Profile Monitor (MWPM) with SiC wires for beam diagnostic along proton beam transport. (**a**) Photograph of MWPC assembled in a chamber; (**b**) Photograph of the chamber containing MWPC installed in the proton beam transport line; (**c**) Photograph of a MWPM frame on which 31 wires of SiC are installed in both horizontal and vertical direction.

5.2.3. Proton Beam Window

To separate ultrahigh vacuum environment in the proton beam transport line from the helium environment in the helium vessel at the target station, a proton beam window (PBW) [69] is placed at 1.8 m upstream of the mercury target. Figure 19 shows a schematic of the PBW. It is made of double walled aluminum alloy of Al5083 with a thickness of 5 mm in total. Al5083 has good characteristics similar to $AlMg_3$ that is used as a safety hull for the 1 MW spallation neutron target at PSI [70], and gives low influence on the scattering of proton beam there. The PBW is replaced every 2 years [69] due to radiation embrittlement. It was estimated that the integral amount of hydrogen produced in Al5083 at the 1 MW proton beam might be equivalent to the total amount produced at the safety hull of PSI. Since the PBW is highly activated after the beam operation, the replacement operation is performed with remote handling tools. Considering the remote handling procedure, an inflatable seal with metal membrane, called pillow seal that was developed by KEK hadron group, is applied to the vacuum seal. Thanks to its good seal performance, very low pressure of less than 10^{-6} Pa has been achieved in the proton beam duct [71]. As shown in Figure 18, radiation shield made of steel with a height of 4 m is connected to the PBW. After the beam operation, the radiation dose rate is lower than 0.2 mSv/h at the flange on the top which is located on the same height as the top of the target station. Access to piping works can be performed by human hands. After removing pipes, the PBW can be plugged out by a crane and pulled into a massive shield cask, and then transferred to the hot cell. In the hot cell, the shielding for the PBW is detached by a remote handing manipulator, and installed on the new PBW. For the reduction of radiation waste volume, water pipes and monitor cables for the PBW are cut by a cutting device placed in the hot cell.

The beam monitors were also assembled to the PBW to observe the characteristics of the beam delivered to the mercury target during the operating period. As shown in Figure 19, the beam monitor, MWPM, was placed at the vacuum side of the PBW. The present SiC wires of MWPC are exposed to the intense proton beams, but it sustained in good conditions until the PBW is replaced. To observe the beam halo at the vicinities of the mercury target, two kinds of beam halo monitors were also placed at the PBW: one is a secondary electron emission type (SEM) to measure relative intensity and the other is a thermocouple type (TC) to measure the intensity quantitatively.
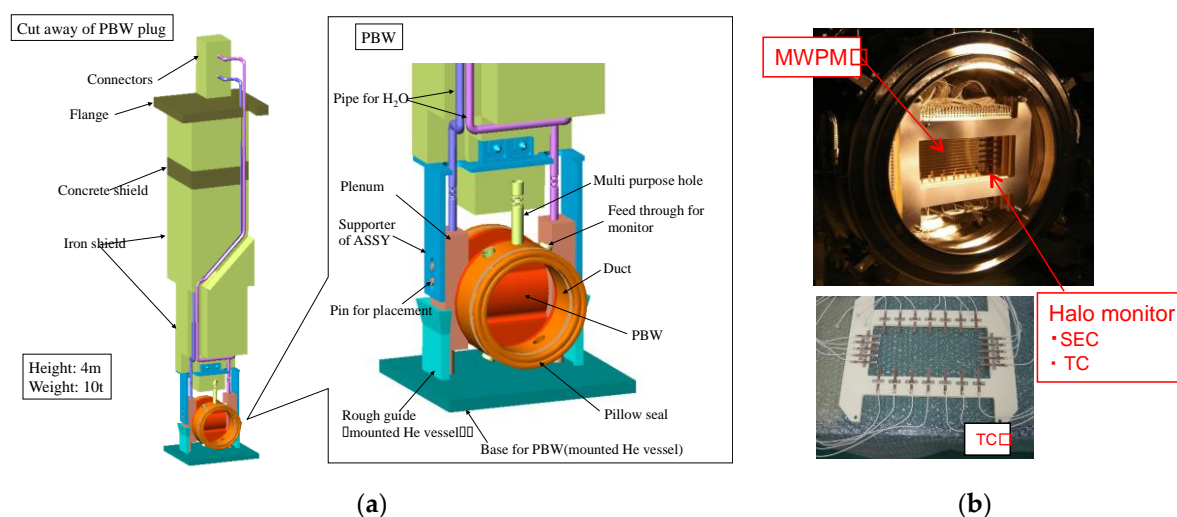

Figure 19. (**a**) Schematic drawing of proton beam window (PBW); (**b**) Beam monitor of MWPM and halo monitor consisting of a secondary electron emission counter (SEC) and thermo couples (TC) placed at the PBW.

5.3. Non-Linear Beam Optics for Mitigation of Cavitation Erosion at the Target Vessel

As increasing the beam power, the cavitation erosion at the mercury target vessel due to the proton beam pulse becomes prominent issues for the lifetime of the target vessel. It is reported that the cavitation erosion at the mercury target vessel is correlated with the proton beam power [72] and the peak current density [22,73]. By changing field of the quadrupole magnet placed in front of the target to enlarge the beam size, the density can be easily decreased, while it causes the increase of heat deposition at the vicinities of the target such as shield, reflector and moderator. Since the cavitation erosion is caused in very short time for each beam shot, an ordinary scanning technique such as pulse bending magnet to obtain flat shape on average is useless to mitigate the erosion. To decrease peak current density sustaining low intensity at the vicinities, nonlinear beam optics with octupole magnets has been developed. Two octupole magnets were placed at upstream of the muon production target (MTG). Due to high order of magnetic field, the beam is shaped to flat distribution [74]. Figure 20 compares the beam shape obtained with nonlinear optics with the experimental results. It is shown that the calculated result is in good agreement with the experimental one even if the proton beam is injected on the muon production target. By introducing nonlinear optics, the peak current density can decrease about 30%, which can be thought to mitigate the pitting erosion effectively.
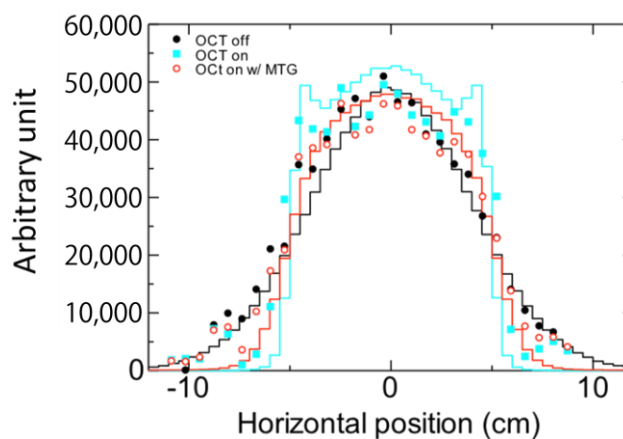
Figure 20. Proton beam profile with nonlinear optics caused by the octupole magnets. Dots stand for the experimental data observed by the MWPM placed at PBW as shown black, cyan and red symbols for results linear optics, nonlinear optics and nonlinear optics with muon production target denoted as muon production target (MTG), respectively. Red, cyan and black lines show calculations with same colors of the experiment.

6. Concluding Remarks

The pulsed spallation neutron source of J-PARC received its very first proton beam from the accelerators in May 2008, and commenced user operation in December 2008. It was measured at a low power operation that a remarkably high neutron intensity of 4.5×10^{12} n/cm^2/s/sr could be emitted from the coupled moderator surface for the 1 MW operation, and a superior resolution of $\Delta d/d = 0.035\%$ was achieved at the beamline BL08 with the poisoned moderator, where d is the lattice-spacing of the Si-400 reflection at 4.628 Å^{-1}. At 300 kW operation, the promising result the pressure wave generated in mercury, could be mitigated to one-third when gas micro-bubbles injection was obtained. In January 2015, the neutron production mercury target received the 1 MW equivalent proton beam pulse for the first time. The beam power for the user program remained still 500 kW so far. Further efforts will be made towards the goal to operate the mercury target system with a beam power of 1 MW.

Noboru Watanabe for his strong support throughout the execution of this work. His enthusiasm, insights and experience was essential for our design of the high-performance target-moderator-reflector system. The authors also appreciate Guenter Bauer, Tim Broome, Jack Carpenter, Hayo Heyck, Hiroaki Kurishita and Tom McManamy for t plenty of useful advice as our formal technical advisory committee. Their advice helped us to make decisions on the component design. Dave Felde, Bob Sangrey, Bernie Riemer and Mark Wendel are also acknowledged for their useful discussions and collaboration on the pressure wave mitigation in the mercury target. The authors are grateful to Takashi Kato for his leadership in the facility construction period and his support until he retired in 2015 and also to Shin-ichi Sakamoto for his significant contribution to the proton beam transport system from the beginning of design until he retired in 2013. They are indebted to Hideki Tatsumoto for his substantial contribution to the design of cryogenic hydrogen system. Finally, the authors also acknowledge the entire neutron source section team, persons involved in the design and construction of this spallation neutron source for their contributions.

Author Contributions: The draft of Sections 1 and 6 was prepared by H.T.; Section 2 by K.H., H.K., T.N. T.W. and M.F.; Section 3 by M.T., M.O., and M.H.; Section 4 by T.A.; Section 5 by S.-I.M., respectively according to their expertizes and primary fields of contribution to the Pulsed Spallation Neutron Source; Revision of the entire draft for integration into the final production was made by H.T.

Conflicts of Interest: The authors declare no conflicts of interest.

References

1. Sakamoto, S. Technical design report of spallation neutron source facility in J-PARC. In *Neutron Source Section*; JAEA-Technology 2011-035; Japan Atomic Energy Agency: Tokai, Japan, 2012.

2. Sakamoto, S.; Meigo, S.; Fujimori, H.; Harada, M.; Konno, C.; Kasugai, Y.; Kai, T.; Miyake, Y.; Ikeda, Y. Advanced design of high-intensity beam transport line in J-PARC. *Nucl. Instrum. Methods Phys. Res. A* **2006**, *562*, 638–641. [CrossRef]

3. Meigo, S.; Noda, F.; Ishikura, S.; Futakawa, M.; Sakamoto, S.; Ikeda, Y. Evaluation of the 3-GeV proton beam profile at the spallation target of the JSNS. *Nucl. Instrum. Methods Phys. Res. A* **2006**, *562*, 569–572. [CrossRef]

4. Meigo, S.; Ooi, M.; Kai, T.; Ono, T.; Ikezaki, K.; Haraguchi, T.; Fujimori, H.; Sakamoto, S. Beam commissioning for neutron and muon facility at J-PARC. *Nucl. Instrum. Methods Phys. Res. A* **2009**, *600*, 41–43. [CrossRef]

5. Yamazaki, Y. *Accelerator Group JAERI/KEK Joint Project Team, Accelerator Technical Design Report for High-Intensity Proton Accelerator Facility Project, J-PARC*; KEK-Report 2002-13; JAERI-Tech 2003-044; Japan Atomic Energy Agency: Tokai, Ibaraki, Japan, 2003.

6. Ohmori, C.; Ezura, E.; Hashimoto, Y.; Mori, Y.; Schnase, A.; Takagi, A.; Uesugi, T.; Yoshii, M.; Tamura, F.; Yamamoto, M. High field gradient cavity for JAERI-KEK joint project. In Proceedings of the 8th European Particle Accelerator Conference (EPAC 2002), Paris, France, 3–7 June 2002; Laclare, J.-L., Ed.; The European Physical Society Interdivisional Group on Accelerators (EPS-IGA) and CERN: Geneva, Switzerland, 2002; pp. 257–259.

7. Tamura, M.; Maekawa, F. *3-Dimensional Shielding Design for a Spallation Neutron Source Facility in the High Intensity Proton Accelerator Project*; JAERI-Tech 2003-010; Japan Atomic Energy Agency: Tokai, Ibaraki, Japan, 2003. (In Japanese)

8. Teshigawara, M.; Kinoshita, H.; Wakui, T.; Meigo, S.; Seki, M.; Ito, M.; Suzuki, T.; Ikezaki, K.; Maekawa, F.; Futakawa, M.; et al. *Maintenance of Used Components in Spallation Neutron Source, Moderator Reflector and Proton Beam Window*; JAEA-Technology 2012-024; Japan Atomic Energy Agency: Tokai, Ibaraki, Japan, 2012.

9. Haines, J.R.; McManamy, T.J.; Gabriel, T.A.; Battle, R.E.; Chipley, K.K.; Crabtree, J.A.; Jacobs, L.L.; Lousteau, D.C.; Rennich, M.J.; Riemer, B.W. Spallation neutron source target station design, development and commissioning. *Nucl. Instrum. Methods Phys. Res. A* **2014**, *764*, 94–115. [CrossRef]

10. Home page of European Spallation Source. Available online: https://europeanspallationsource.se/european-spallation-source (accessed on 25 July 2017).

11. Kaminaga, M.; Terada, A.; Haga, K.; Kinoshita, H.; Ishikura, S.; Hino, R. *Study of Integrated Structure of Mercury Target Container with Safety Hull*; JAERI-Tech 2000-076; Japan Atomic Energy Agency: Tokai, Ibaraki, Japan, 2001.

12. Futakawa, M.; Kogawa, H.; Hino, R. Measurement of dynamics response of liquid metal subjected to uniaxial strain wave. *J. Phys. IV Fr.* **2000**, *10*, Pr9-237–Pr9-242. [CrossRef]

13. Futakawa, M.; Naoe, T.; Kogawa, H.; Tsai, C.C.; Ikeda, Y. Pitting damage formation up to over 10 million cycles off-line test by MIMTM. *J. Nucl. Sci. Technol.* **2003**, *40*, 895–904. [CrossRef]

14. Naoe, T.; Futakawa, M. Pressure wave-induced cavitation erosion in narrow channel of stagnant mercury. *Trans. JSME* **2014**, *80*, fe0025-1-12. (In Japanese) [CrossRef]

15. Okita, K.; Takagi, S.; Matsumoto, Y. Propagation of pressure waves, caused by a thermal shock, in liquid metals containing gas bubbles. *J. Fluid Sci. Technol.* **2008**, *3*, 116–128. [CrossRef]

16. Futakawa, M.; Kogawa, H.; Hasegawa, S.; Naoe, T.; Ida, M.; Haga, K.; Wakui, T.; Tanaka, N.; Matsumoto, Y.; Ikeda, Y. Mitigation technologies for damage induced by pressure waves in high-power mercury spallation neutron sources (II) bubbling effect to reduce pressure wave. *J. Nucl. Sci. Technol.* **2008**, *45*, 1041–1048. [CrossRef]

17. Kogawa, H.; Naoe, T.; Kyotoh, H.; Haga, K.; Kinoshita, H.; Futakawa, M. Development of microbubble generator for suppression of pressure waves in mercury target of spallation source. *J. Nucl. Sci. Technol.* **2015**, *52*, 1461–1469. [CrossRef]

18. Kinoshita, H.; Haga, K.; Kaminaga, M.; Hino, R. Experiments on mercury circulation system for spallation neutron target. *J. Nucl. Sci. Technol.* **2004**, *41*, 376–384. [CrossRef]

19. Kogawa, H.; Haga, K.; Wakui, T.; Futakawa, M. Development on mercury pump for JSNS. *Nucl. Instrum. Methods Phys. Res. A* **2009**, *600*, 97–99. [CrossRef]

20. Futakawa, M.; Kogawa, H.; Hasegawa, S.; Ikeda, Y.; Riemer, B.; Wendel, M.; Haines, J.; Bauer, G.; Naoe, T.; Okita, K.; et al. Cavitation damage prediction for spallation target vessels by assessment of acoustic vibration. *J. Nucl. Mater.* **2008**, *377*, 182–188. [CrossRef]

21. Teshigawara, M.; Wakui, T.; Naoe, T.; Kogawa, H.; Maekawa, F.; Futakawa, M.; Kikuchi, K. Development of JSNS target vessel diagnosis system using laser Doppler method. *J. Nucl. Mater.* **2010**, *398*, 238–243. [CrossRef]

22. Kogawa, H.; Naoe, T.; Futakawa, M.; Haga, K.; Wakui, T.; Harada, M.; Takada, H. Mitigation technologies for damage induced by pressure waves in high-power mercury spallation neutron source (IV)—Measurement on pressure wave response and microbubble effect on mitigation in JSNS mercury target. *J. Nucl. Sci. Technol.* **2017**, *54*, 733–741. [CrossRef]

23. Kai, T.; Kasugai, Y.; Ooi, M.; Kogawa, H.; Haga, K.; Kinoshita, H.; Seki, M.; Harada, M. Experiences on radioactivity handling for mercury target system in MLF/J-PARC. *Prog. Nucl. Sci. Technol.* **2014**, *4*, 380–383. [CrossRef]

24. Teshigawara, M.; Watanabe, N.; Takada, H.; Nakashima, H.; Nagao, T.; Oyama, Y.; Kosako, K. *Neutronic Studies of Bare Targets for JAERI 5 MW Pulsed Spallation Neutron Source*; JAERI-Research 99-010; Japan Atomic Energy Agency: Tokai, Ibaraki, Japan, 1999.

25. Teshigawara, M.; Harada, M.; Watanabe, N.; Kai, T.; Sakata, A.; Ikeda, Y.; Ooi, M. Proton energy dependence of slow neutron intensity. In Proceedings of the Fifteenth Meeting of the International Collaboration on Advanced Neutron Sources ICANS-XV, Tsukuba, Japan, 6–9 November 2000; Suzuki, J., Itoh, S., Eds.; Japan Atomic Energy Research Institute: Ibaraki, Japan, 2001; pp. 835–847.

26. Broome, T.A.; Hogston, J.R.; Holding, M.; Howells, W.S. The isis methane moderator. In Proceedings of the Twelfth Meeting of International Collaboration on Advanced Neutron Sources, Abingdon, Oxfordshire, UK, 24–28 May 1993; Steigenberger, U., Broome, T., Rees, G., Soper, A., Eds.; Rutherford Appleton Laboratory: Oxfordshire, UK, 1994; pp. T156–T163.

27. Scott, T.L.; Carpenter, J.M.; Miller, M.E. The development of solid methane neutron moderators at the intense pulsed neutron source facility of Argonne National Laboratory. In Proceedings of the International Workshop on Cold Moderators for Pulsed Neutron Sources, Argonne National Laboratory, Lemont, IL, USA, 29 September–2 October 1997; Carpenter, J.M., Iverson, E.B., Eds.; 1997; pp. 299–304. Available online: http://www.osti.gov/scitech/biblio/12385/ (accessed on 25 July 2017).

28. Ishikawa, Y.; Ikeda, S.; Watanabe, N.; Kondo, K.; Inoue, K.; Kiyanagi, Y.; Iwasa, H.; Tsuchihashi, K. Grooved cold moderator at KENS. In Proceedings of the Seventh Meeting of the International Collaboration on Advanced Neutron Sources ICANS-VII, Chalk River, Ontario, ON, Canada, 13–16 September 1983; Schriber, O.S., Ed.; Chalk River Nuclear Laboratories: Ontario, ON, Canada, 1984; pp. 230–235.

29. MacFarlane, R.E. *New Thermal Neutron Scattering Files for ENDF/B-VI Release 2*; LA-12639-MS; Los Alamos National Laboratory Report: Los Alamos, NM, USA, March 1994.

30. Kiyanagi, Y.; Watanabe, N.; Iwasa, H. Premoderator studies for a coupled liquid-hydrogen moderator in pulsed spallation neutron sources. *Nucl. Instrum. Methods Phys. Res. A* **1994**, *343*, 558–562. [CrossRef]

31. Kai, T.; Teshigawara, M.; Watanabe, N.; Harada, M.; Sakara, H.; Ikeda, Y. Optimization of coupled hydrogen moderator for a short pulse spallation neutron source. *J. Nucl. Sci. Technol.* **2002**, *39*, 120–128. [CrossRef]

32. Harada, M.; Teshigawara, M.; Kai, T.; Sakata, H.; Watanabe, N.; Ikeda, Y. Neutronic optimization of premoderator and reflector for decoupled hydrogen moderator in 1 MW spallation neutron source. *J. Nucl. Sci. Technol.* **2002**, *39*, 827–837. [CrossRef]

33. Watanabe, N.; Harada, M.; Kai, T.; Teshigawara, M.; Ikeda, Y. Optimization of coupled and decoupled moderators for a short pulse spallation source. *J. Neutron Res.* **2013**, *11*, 13–23. [CrossRef]

34. Harada, M.; Teshigawara, M.; Watanabe, N.; Kai, T.; Ikeda, Y. Optimization of poisoned and unpoisoned decoupled moderators in JSNS. In Proceedings of the Sixteenth Meeting of the International Collaboration on Advanced Neutron Sources (ICANS XVI), Düsseldorf-Neuss, Germany, 12–15 May 2003; Mank, G., Conrad, H., Eds.; Forschungszentrum Jülich GmbH: Jülich, Germany, 2003; pp. 697–706.

35. Kai, T.; Harada, M.; Teshigawara, M.; Watanabe, N.; Ikeda, Y. Coupled hydrogen moderator optimization with ortho/para hydrogen ratio. *Nucl. Instrum. Methods Phys. Res. A* **2004**, *523*, 398–414. [CrossRef]

36. Kai, T.; Harada, M.; Teshigawara, M.; Watanabe, N.; Kiyanagi, Y.; Ikeda, Y. Neutronic performance of rectangular and cylindrical coupled hydrogen moderators in wide-angle beam extraction of low-energy neutrons. *Nucl. Instrum. Methods Phys. Res. A* **2005**, *550*, 329–342. [CrossRef]

37. Kai, T.; Harada, M.; Teshigawara, M.; Watanabe, N.; Ikeda, Y. Neutronic study on coupled hydrogen moderator for J-PARC spallation neutron source. In Proceedings of the Sixteenth Meeting of the International Collaboration on Advanced Neutron Sources (ICANS XVI), Düsseldorf-Neuss, Germany, 12–15 May 2003; Mank, G., Conrad, H., Eds.; Forschungszentrum Jülich GmbH: Jülich, Germany, 2003; pp. 657–666.

38. Harada, M.; Watanabe, N.; Teshigawara, M.; Kai, T.; Ikeda, Y. Neutronic studies on decoupled hydrogen moderator for a short-pulse spallation source. *Nucl. Instrum. Methods Phys. Res. A* **2005**, *539*, 345–362. [CrossRef]

39. Harada, M.; Watanabe, N.; Teshigawara, M.; Kai, T.; Kato, T.; Ikeda, Y. Neutronics of a poisoned para-hydrogen moderator for a pulsed spallation neutron source. *Nucl. Instrum. Methods Phys. Res. A* **2007**, *574*, 407–419. [CrossRef]

40. Maekawa, F.; Harada, M.; Oikawa, K.; Teshigawara, M.; Kai, T.; Meigo, S.; Ooi, M.; Sakamoto, S.; Takada, H.; Futakawa, M.; et al. First neutron production utilizing J-PARC pulsed spallation neutron source JSNS and neutronic performance demonstrated. *Nucl. Instrum. Methods Phys. Res. A* **2010**, *620*, 159–165. [CrossRef]

41. Batkov, K.; Takibayev, A.; Zanini, L.; Mezei, F. Unperturbed moderator brightness in pulsed neutron sources. *Nucl. Instrum. Methods Phys. Res. A* **2013**, *729*, 500–505. [CrossRef]

42. Mezei, F.; Zanini, L.; Takibayev, A.; Batkov, K.; Klinkby, E.; Pitcher, E.; Schronfeldt, T. Low dimensional neutron moderators for enhanced source brightness. *J. Neutron Res.* **2014**, *17*, 101–105. [CrossRef]

43. Gallmeier, F.X.; Lu, W.; Riemer, B.W.; Zhao, J.K.; Herwig, K.W. Conceptual moderator studies for the spallation neutron source short-pulse second target station. *Rev. Sci. Instrum.* **2016**, *87*, 063304. [CrossRef] [PubMed]

44. Iverson, E.B.; Carpenter, J.M. Kinetics of irradiated liquid hydrogen. In Proceedings of the 6th International Workshop on Advanced Cold Moderators (ACoM-6), Jülich, Germany, 11–13 September 2002; Conrad, H., Ed.; Forschungszentrum Jülich GmbH: Jülich, Germany, 2002; pp. 51–58.

45. Iverson, E.B.; Carpenter, J.M. Kinetics of irradiated liquid hydrogen. In Proceedings of the Sixteenth Meeting of the International Collaboration on Advanced Neutron Sources (ICANS XVI), Düsseldorf-Neuss, Germany, 12–15 May 2003; Mank, G., Conrad, H., Eds.; Forschungszentrum Jülich GmbH: Jülich, Germany, 2003; pp. 707–718.

46. Ooi, M.; Ogawa, H.; Kamiyama, T.; Kiyanagi, Y. Experimental studies of the effect of the ortho/para ratio on the neutronic performance of a liquid hydrogen moderator for a pulsed neutron source. *Nucl. Instrum. Methods Phys. Res. A* **2011**, *659*, 61–68. [CrossRef]

47. Ooi, M.; Ino, T.; Muhrer, G.; Pitcher, E.J.; Russell, G.J.; Ferguson, P.D.; Iverson, E.B.; Freeman, D.; Kiyanagi, Y. Measurements of the change of neutronic performance of a hydrogen moderator at Manuel Lujan Neutron Scattering Center due to conversion from orth- to para-hydrogen state. *Nucl. Instrum. Methods Phys. Res. A* **2006**, *566*, 699–705. [CrossRef]

48. Teshigawara, M.; Harada, M.; Tatsumoto, H.; Aso, T.; Ohtsu, K.; Takada, H.; Futakawa, M.; Ikeda, Y. Experimental verification of equilibrium para-hydrogen levels in hydrogen moderations irradiated by spallation neutrons at J-PARC. *Nucl. Instrum. Methods Phys. Res. B* **2016**, *368*, 66–70. [CrossRef]

49. Teshigawara, M.; Harada, M.; Saito, S.; Oikawa, K.; Maekawa, F.; Futakawa, M.; Kikuchi, K.; Kato, T.; Ikeda, Y.; Naoe, T.; et al. Development of aluminum (Al5083)-clad ternary Ag-In-Cd alloy for JSNS decoupled moderator. *J. Nucl. Mater.* **2006**, *356*, 300–307. [CrossRef]

50. Harada, M.; Saito, S.; Teshigawara, M.; Kawai, M.; Kukuchi, K.; Watanabe, N.; Ikeda, Y. Silver-indium-cadmium decoupler and liner. In Proceedings of the Sixteenth Meeting of the International Collaboration on Advanced Neutron Sources (ICANS XVI), Düsseldorf-Neuss, Germany, 12–15 May 2003; Mank, G., Conrad, H., Eds.; Forschungszentrum Jülich GmbH: Jülich, Germany, 2003; pp. 677–687.

51. Teshigawara, M.; Harada, M.; Saito, S.; Kikkuchi, K.; Kogawa, H.; Kawai, M.; Kurishita, H.; Konashi, K. Cladding technique for development of Ag-In-Cd decoupler. *J. Nucl. Mater.* **2005**, *343*, 154–162. [CrossRef]

52. Kikuchi, K.; Teshigawara, M.; Harada, M.; Saito, S.; Maekawa, F.; Futakawa, M.; Ishigaki, T. A challenge for a high-resolution Ag-In-Cd decoupler in intensified short-pulsed neutron source. *Mater. Sci. Forum* **2010**, *652*, 92–98. [CrossRef]

53. Harada, M.; Teshigawara, M.; Maekawa, F.; Futakawa, M. Study on low activation material for MW-Class spallation neutron sources. *J. Nucl. Mater.* **2010**, *398*, 93–99. [CrossRef]

54. Ooi, M.; Teshigawara, M.; Wakui, T.; Nishi, T.; Harada, M.; Maekawa, F.; Futakawa, M. Development status of low activation ternary Au-In-Cd alloy decoupler for a MW class spallation neutron source: 1st Production of Au-In-Cd alloy. *J. Nucl. Mater.* **2012**, *431*, 218–223. [CrossRef]

55. Ooi, M.; Teshigawara, M.; Kai, T.; Harada, M.; Maekawa, F.; Futakawa, M.; Hashimoto, E.; Segawa, M.; Kureta, M.; Tremsin, A.; et al. Neutron resonance imaging of a Au-In-Cd alloy for the JSNS. *Phys. Procedia* **2013**, *43*, 337–342. [CrossRef]

56. Ooi, M.; Teshigawara, M.; Harada, M.; Naoe, T.; Maekawa, F.; Kasugai, Y. Development of Au-In-Cd decoupler by a hot isostatic pressing (HIP) technique for short pulsed spallation neutron source. *J. Nucl. Mater.* **2014**, *450*, 117–122. [CrossRef]

57. Kamiyama, T.; Oikawa, K. Powder diffractometer at J-PARC. In Proceedings of the Sixteenth Meeting of the International Collaboration on Advanced Neutron Sources (ICANS XVI), Dusseldorf-Neuss, Germany, 12–15 May 2003; Mank, G., Conrad, H., Eds.; Forschungszentrum Jülich GmbH: Jülich, Germany, 2003; pp. 309–314.

58. Aso, T.; Tatsumoto, H.; Hasegawa, S.; Ushijima, I.; Ohtsu, K.; Kato, T.; Ikeda, Y. Design result of the cryogenic hydrogen circulation system for 1 MW pulse spallation neutron source (JSNS) in J-PARC. *AIP Conf. Proc.* **2006**, *823*, 763–770. [CrossRef]

59. Aso, T.; Tatsumoto, H.; Hasegawa, S.; Ohtsu, K.; Uehara, T.; Kawakami, Y.; Sakurayama, H.; Maekawa, F.; Futakawa, M.; Ushijima, I. Commissioning of the cryogenic hydrogen system in J-PARC: Preliminary operation by helium gas. In Proceedings of the Twenty-Second International Cryogenic Engineering Conference and International Cryogenic Materials Conference 2008, Seoul, Korea, 21–25 July 2008; Korea Institute of Applied Superconductivity and Cryogenics: Seoul, Korea, 2009; pp. 741–746.

60. Tatsumoto, H.; Aso, T.; Kato, T.; Ohtsu, K.; Hasegawa, S.; Maekawa, F.; Futakawa, M. Commissioning of the cryogenic hydrogen system in J-PARC: First cool-down operation with helium. In Proceedings of the Twenty-Second International Cryogenic Engineering Conference and International Cryogenic Materials Conference 2008, Seoul, Korea, 21–25 July 2008; Korea Institute of Applied Superconductivity and Cryogenics: Seoul, Korea, 2009; pp. 717–722.

61. Miyake, Y.; Shimomura, K.; Kawamura, N.; Strasser, P.; Makimura, S.; Koda, A.; Fujimori, H.; Nakahara, K.; Kadono, R.; Kato, M.; et al. Birth of an intense pulsed muon source, J-PARC MUSE. *Physica B* **2009**, *404*, 957–961. [CrossRef]

62. Higemoto, W.; Kadono, R.; Kawamura, N.; Koda, A.; Kojima, K. M.; Makimura, S.; Matoba, S.; Miyake, Y.; Shimomura, K.; Strasser, P. Materials and Life Science Experimental Facility at the Japan Proton Accelerator Research Complex IV: The Muon Facility. *Quantum Beam Sci.* **2017**, *1*, 11. [CrossRef]

63. Fujimori, H.; Kawamura, N.; Meigo, S.; Strasser, P.; Nakahara, K.; Miyake, Y. Radiation resistant magnets for the J-PARC muon facility. *Nucl. Instrum. Methods Phys. Res. A* **2009**, *600*, 170–172. [CrossRef]

64. Meigo, S.; Ooi, M.; Ikezaki, K.; Akutsu, A.; Sakamoto, S.; Futakawa, M. Development of profile monitor system for high intense spallation neutron source. In Proceedings of the 1st International Beam Instrumentation Conference, IBIC 2012, Tsukuba, Japan, 1–4 October 2012; Mitsuhashi, T., Shirakawa, A., Eds.; JACow: Geneva, Switzerland, 2013; pp. 227–231. Available online: http://epaper.kek.jp/IBIC2012/papers/mopb68.pdf/ (accessed on 25 July 2017).

65. Sakai, K.; Kai, T.; Ooi, M.; Watanabe, A.; Nakatani, T.; Higemoto, W.; Meigo, S.; Sakamoto, S.; Takada, H.; Futakawa, M. Operation status of interlock system of Materials and Life Science Experimental Facility (MLF) in J-PARC. *Prog. Nucl. Sci. Technol.* **2014**, *4*, 264–267. [CrossRef]

66. Home Page of Experimental Physics and Industrial Control System (EPICS). Available online: http://www.aps.anl.gov/epics/ (accessed on 5 July 2017).

67. Ooi, M.; Kai, T.; Meigo, S.; Kinoshita, H.; Sakai, K.; Sakamoto, S.; Kaminaga, M.; Katoh, T.; Katoh, T. Development of beam monitor DAQ system for 3NBT at J-PARC. In Proceedings of the 10th ICALEPCS International Conference on Accelerator and Large Experiment Physical Control System, Geneva, Switzerland, 10–14 October 2005; PO1.024. pp. 1–6. Available online: http://accelconf.web.cern.ch/accelconf/ica05/proceedings/pdf/P1_024.pdf/ (accessed on 25 July 2017).

68. Home Page of Strategic Accelerator Design (SAD). Available online: http://acc-physics.kek.jp/SAD/ (accessed on 25 July 2017).

69. Meigo, S.; Ooi, M.; Harada, M.; Kinoshita, H.; Akutsu, A. Radiation damage and lifetime estimation of the proton beam window at the Japan Spallation Neutron Source. *J. Nucl. Mater.* **2014**, *450*, 141–146. [CrossRef]

70. Dai, Y.; Hamaguchi, D. Mechanical properties and microstructure of $AlMg_3$ irradiated in SINQ Target-3. *J. Nucl. Mater.* **2005**, *343*, 184–190. [CrossRef]

71. Saito, Y.; Naito, F.; Kubota, C.; Meigo, S.; Fujimori, H.; Ogiwara, N.; Kamiya, J.; Kinsho, M.; Kabeya, Z.; Kubo, T.; et al. Material and surface processing in J-PARC vacuum system. *Vacuum* **2012**, *86*, 817–821. [CrossRef]

72. McClintock, D.A.; Riemer, B.W.; Ferguson, P.D.; Carroll, A.J.; Dayton, M.J. Initial observations of cavitation-induced erosion of liquid metal spallation target vessels at the Spallation Neutron Source. *J. Nucl. Mater.* **2012**, *431*, 147–159. [CrossRef]

73. Naoe, T.; Xiong, Z.; Futakawa, M. Gigacycle fatigue behavior of austenitic stainless steels used for mercury target vessels. *J. Nucl. Mater.* **2016**, *468*, 331–338. [CrossRef]

74. Meigo, S.; Ooi, M.; Ikezaki, K.; Akutsu, A. Beam flattening system based on non-linear optics for high power spallation neutron target at J-PARC. In Proceedings of the 5th International Particle Accelerator Conference, (IPAC2014), Dresden, Germany, 15–20 June 2014; Petit-Jean-Genaz, C., Arduini, G., Michel, P., Schaa, V.R.W., Eds.; JACow: Geneva, Switzerland, 2014; pp. 896–898. Available online: http://accelconf.web.cern.ch/AccelConf/IPAC2014/papers/mopri116.pdf/ (accessed on 25 July 2017).